Cavendish-HEP-02/16
NIKHEF/2002-014
ITP-2002/62
DESY 02-216
LBNL-51590
February 1, 2008

Threshold Effects in Charm Hadroproduction

Nikolaos Kidonakis[a], Eric Laenen[b], Sven Moch[c], Ramona Vogt[d]

[a] *Cavendish Laboratory*
University of Cambridge, Cambridge CB3 0HE, UK

[b] *NIKHEF Theory Group*
P.O. Box 41882, 1009 DB Amsterdam, The Netherlands
and
Institute for Theoretical Physics
Utrecht University, Utrecht, The Netherlands

[c] *Deutsches Elektronensynchrotron*
DESY Platanenallee 6, D–15738 Zeuthen, Germany

[d] *Nuclear Science Division,*
Lawrence Berkeley National Laboratory, Berkeley, CA 94720, USA
and
Physics Department,
University of California at Davis, Davis, CA 95616, USA

Abstract

We describe calculations of $c\overline{c}$ production to next-to-next-to-leading order (NNLO) and next-to-next-to-leading logarithm (NNLL) near threshold in pp and $\pi^- p$ interactions. We study the relevance of these calculations for existing $c\overline{c}$ total cross section data by examining their sensitivity to partonic threshold kinematics, their convergence properties and scale dependence.

1 Introduction

Calculations of charm production are still not under solid theoretical control. A good understanding of the charm cross section is of particular interest for heavy ion physics. Charm production is an important contribution to the dilepton continuum in heavy ion collisions. In S+U and Pb+Pb interactions at the CERN SPS, with $\sqrt{S} = 19.4$ and 17.3 GeV/nucleon pair[1] respectively, the dilepton yield in the mass range $1.5 < m_{\mu^+\mu^-} < 2.5$ GeV is enhanced by a factor of 2-3 over the extrapolated proton-nucleus, pA, yield [1]. These data have been interpreted as an enhancement of the charm production cross section in the system created in the heavy ion collision. Another possible source of the dilepton enhancement is thermal dilepton production, predicted in a quark-gluon plasma [2]. Finally, the total charm rate would be a useful reference for J/ψ production in heavy ion collisions [2, 3, 4].

Although many future heavy ion experiments will be at high collider energies, $\sqrt{S} \geq 130$ GeV, some of the current and future experiments, like those at the SPS, are in the near-threshold region. The NA60 experiment was specifically designed to distinguish between charm decays and Drell-Yan-like production of dileptons [5] to determine the cause of the apparent enhancement. It will take heavy ion data at $\sqrt{S} = 17.3$ GeV and pA data at $\sqrt{S} = 29.1$ GeV. A new facility is being built at the GSI [6] that will measure charm near threshold with $\sqrt{S} = 6.98$ GeV.

Because the charm quark mass is a few times $\Lambda_{\rm QCD}$, it is generally treated as a heavy quark in perturbative QCD calculations. However, its relative lightness results in a rather strong dependence of the total cross section on mass and scale, with up to a factor of 100 between the lowest and highest next-to-leading order (NLO) results [7]. There is also a rather broad spread in the measured charm production cross section data at fixed target energies. Much of this uncertainty arises from low statistics in the early experiments, assumptions of how much of the total charm yield results in final-state D mesons, and how the measured data are extrapolated to full phase space. The more recent data have improved considerably with new detection techniques and higher statistics.

Improvements in the calculation of the charm cross section are difficult at all energies, but are perhaps possible when the $c\overline{c}$ pair is produced close to threshold, as we now describe. Factorization properties of QCD separate cross sections into universal, nonperturbative parton densities and a perturbatively calculable hard scattering function, the partonic cross section. Remnants of long-distance dynamics in the hard scattering function can dominate corrections at higher orders near production threshold. These Sudakov corrections have the form of distributions singular at partonic threshold. Threshold resummation techniques organize these singular distributions to all orders, presumably extending the reach of QCD into near-threshold production. The singular functions organized by resummation are plus distributions, of the form $[\ln^l x/x]_+$, where x denotes the 'distance' from partonic threshold. At next-to-leading log (NLL) accuracy and beyond, proper account must be taken of the color structure of the hard scattering [8, 9] for each partonic subprocess.

Resummed cross sections are useful as generating functions for approximate finite order corrections to the cross section when expanded in powers of the strong coupling constant α_s, as we do in this paper. The resummed cross sections may also be evaluated numerically. The charm fixed-target data were first compared to a leading log (LL) resummed calculation of the

[1]Unless otherwise specified, all pA energies are per nucleon and nucleus-nucleus energies are per nucleon pair.

total cross section in Ref. [10]. Because the ratio m/Λ_3 is quite small, the expansion parameter, α_s, is not and the LL resummation began to fail at $\sqrt{S} \approx 20$ GeV. A NLL resummed evaluation in Ref. [11] found significant threshold corrections, albeit with a reduction in scale dependence.

In this paper we work at finite order, using our results of Refs. [12, 13]. We have calculated the double-differential heavy quark hadroproduction cross sections up to next-to-next-to-leading order (NNLO), $\mathcal{O}(\alpha_s^4)$, and next-to-next-to-leading logarithm (NNLL), *i.e.* keeping powers of the singular functions as low as $l = 2i-1$ at order $\mathcal{O}(\alpha_s^{i+3})$ where $i = 0, 1, \ldots$ [12, 13]. We only discuss $Q\overline{Q}$ production in the $ij = q\overline{q}$ and gg channels since qg scattering first appears at NLO.

Our studies focus on the kinematics of the proposed GSI facility and the CERN SPS proton and ion fixed target programs. We first briefly describe our NNLO-NNLL calculations in the next section. In section 3 we discuss whether the ion beam energies will actually produce charm in the near-threshold region where our calculations are in principle applicable. We show results for several values of the charm quark mass, $m = 1.2$, 1.5 and 1.8 GeV and for scales $\mu = m$ and $2m$. We compare our results for the NNLO-NNLL inclusive $c\overline{c}$ cross section to charm production data and to the NLO cross sections in the relevant energy regime, and judge their value. Finally, we summarize our results in section 4.

2 Resummation

In our approach, the distance from partonic threshold in the singular functions depends on how the cross section is calculated. We either integrate over the momentum of the unobserved heavy quark or antiquark and determine the one-particle inclusive (1PI) cross section for the detected quark or treat the Q and $\overline{Q}$ as a pair in the integration, in pair invariant mass (PIM) kinematics. In 1PI kinematics,

$$p(P_1) + p(P_2) \longrightarrow Q(p_1) + X(p_X)\,, \tag{1}$$

where X denotes any hadronic final state containing the heavy antiquark and $Q(p_1)$ is the identified heavy quark. The reaction in Eq. (1) is dominated by the partonic reaction

$$i(k_1) + j(k_2) \quad \longrightarrow \quad Q(p_1) + X[\overline{Q}](p_2')\,. \tag{2}$$

At LO or if $X[\overline{Q}](p_2') \equiv \overline{Q}(\overline{p}_2)$, the reaction is at partonic threshold with $\overline{Q}$ momentum $\overline{p}_2$. At threshold the heavy quarks are not necessarily produced at rest but with equal and opposite momentum. The partonic Mandelstam invariants are

$$s = (k_1 + k_2)^2\,, \quad t_1 = (k_2 - p_1)^2 - m^2\,, \quad u_1 = (k_1 - p_1)^2 - m^2\,, \quad s_4 = s + t_1 + u_1 \tag{3}$$

where the last, $s_4 = (p_2')^2 - m^2$, is the inelasticity of the partonic reaction. At threshold, $s_4 = 0$. Thus the distance from threshold in 1PI kinematics is $x = s_4/m^2$ and the cross sections are functions of t_1 and u_1. In PIM kinematics the pair is treated as a unit so that, on the partonic level, we have

$$i(k_1) + j(k_2) \quad \longrightarrow \quad Q\overline{Q}(p') + X(k')\,. \tag{4}$$

The square of the heavy quark pair mass is $p'^2 = M^2$. At partonic threshold, $X(k') = 0$, the three Mandelstam invariants are

$$s = M^2\,, \quad t_1 = -\frac{M^2}{2}(1 - \beta_M \cos\theta)\,, \quad u_1 = -\frac{M^2}{2}(1 + \beta_M \cos\theta) \tag{5}$$

where $\beta_M = \sqrt{1-4m^2/M^2}$ and θ is the scattering angle in the parton center of mass frame. Now the distance from threshold is $x = 1 - M^2/s \equiv 1 - z$ where $z = 1$ at threshold. In PIM kinematics the cross sections are functions of M^2 and $\cos\theta$.

The resummation is done in moment space by making a Laplace transformation with respect to x, the distance from threshold. Then the singular functions become linear combinations of $\ln^k \tilde{N}$ with $k \leq l+1$ and $\tilde{N} = Ne^{\gamma_E}$ where γ_E is the Euler constant. The 1PI resummed double differential partonic cross section in moment space is

$$s^2 \frac{d^2\sigma_{ij}^{\rm res}(\tilde{N})}{dt_1\, du_1} \;=\; {\rm Tr}\Bigg\{ H_{ij} \bar{\rm P} \exp\left[\int_m^{m/N} \frac{d\mu'}{\mu'} (\Gamma_S^{ij}\,(\alpha_s(\mu')))^\dagger\right] \tilde{S}_{ij} {\rm P} \exp\left[\int_m^{m/N} \frac{d\mu'}{\mu'} \Gamma_S^{ij}\,(\alpha_s(\mu'))\right]\Bigg\} \qquad (6)$$
$$\times \exp\left(\tilde{E}_i(N_u,\mu,\mu_R)\right)\, \exp\left(\tilde{E}_j(N_t,\mu,\mu_R)\right)\, \exp\left\{2\int_{\mu_R}^{m} \frac{d\mu'}{\mu'}\, \left(\gamma_i\,(\alpha_s(\mu')) + \gamma_j\,(\alpha_s(\mu'))\right)\right\},$$

where $N_u = N(-u_1/m^2)$, $N_t = N(-t_1/m^2)$, and $(\overline{\rm P})$ P refer to (anti-)path ordering. To find the PIM result, transform t_1 and u_1 to M^2 and $\cos\theta$ using Eq. (5) and let $N_u = N_t = N$. The cross section depends on the 'hard', H_{ij}, and 'soft', $\tilde{S}_{ij}$, functions which are Hermitian matrices in the space of color exchanges. The 'hard' part contains no singular functions. The 'soft' component contains the singular functions associated with non-collinear soft-gluon emission. The soft anomalous dimension matrix, Γ_S^{ij}, is two dimensional for $q\overline{q}$ and three for gg. The universal Sudakov factors are in the exponents $\tilde{E}_i$, expanded as

$$\exp(\tilde{E}_i(N_u,\mu,m)) \simeq 1 + \frac{\alpha_s}{\pi}\left(\sum_{k=0}^{2} C_k^{i,(1)} \ln^k(N_u)\right) + \left(\frac{\alpha_s}{\pi}\right)^2 \left(\sum_{k=0}^{4} C_k^{i,(2)} \ln^k(N_u)\right) + \ldots\ . \qquad (7)$$

These exponents also contain the effects of the singular functions due to soft-collinear radiation. The coefficients $C_k^{i,(n)}$, as well as the detailed derivation of the resummed and finite-order cross sections, can be found in Ref. [13]. The momentum space cross sections to NNLO-NNLL are obtained by gathering terms at $\mathcal{O}(\alpha_s^3)$ and $\mathcal{O}(\alpha_s^4)$, inverting the Laplace transformation and matching the N-independent terms in H_{ij} and $\tilde{S}_{ij}$ to the exact $\mathcal{O}(\alpha_s^3)$ results in Refs. [14, 15].

Any difference in the integrated cross sections due to kinematics choice arises from the ambiguity of the estimates. At leading order the threshold condition is exact and there is no difference between the total cross sections in the two kinematic schemes. However, beyond LO additional soft partons are produced and there is a difference. To simplify the argument, the total partonic cross section may be expressed in terms of dimensionless scaling functions $f_{ij}^{(k,l)}$ that depend only on $\eta = s/4m^2 - 1$ [13],

$$\sigma_{ij}(s,m^2,\mu^2) = \frac{\alpha_s^2(\mu)}{m^2} \sum_{k=0}^{\infty}\ (4\pi\alpha_s(\mu))^k \sum_{l=0}^{k}\ f_{ij}^{(k,l)}(\eta)\ \ln^l\left(\frac{\mu^2}{m^2}\right). \qquad (8)$$

We have constructed LL, NLL, and NNLL approximations to $f_{ij}^{(k,l)}$ in the $q\overline{q}$ and gg channels for $k \leq 2$, $l \leq k$. Exact results are known for $k = 1$ and can be derived using renormalization group methods for $k = 2$, $l = 1, 2$ [13]. Our calculations use the exact LO and NLO cross sections with the approximate NNLO-NNLL corrections.

The inclusive hadronic cross section is obtained by convoluting the inclusive partonic cross

sections with the parton luminosity Φ_{ij},

$$\Phi_{ij}(\tau,\mu^2) \;=\; \tau \int\limits_0^1 dx_1 \int\limits_0^1 dx_2 \; \delta(x_1 x_2 - \tau) \; \phi_{i/h_1}(x_1,\mu^2)\, \phi_{j/h_2}(x_2,\mu^2)\,, \tag{9}$$

where $\phi_{i/h}(x,\mu^2)$ is the density of partons of flavor i in hadron h carrying a fraction x of the initial hadron momentum, at factorization scale μ. Then

$$\begin{aligned} \sigma_{h_1 h_2}(S,m^2) &= \sum_{i,j=q,\bar{q},g} \int\limits_{4m^2/S}^1 \frac{d\tau}{\tau} \; \Phi_{ij}(\tau,\mu^2) \; \sigma_{ij}(\tau S, m^2, \mu^2) \qquad (10) \\ &= \sum_{i,j=q,\bar{q},g} \int_{-\infty}^{\log_{10}(S/4m^2-1)} d\log_{10}\eta \, \frac{\eta}{1+\eta} \ln(10) \; \Phi_{ij}(\eta,\mu^2) \; \sigma_{ij}(\eta, m^2, \mu^2) \end{aligned}$$

where

$$\eta = \frac{s}{4m^2} - 1 \;=\; \frac{\tau S}{4m^2} - 1\,. \tag{11}$$

Our investigations in Ref. [13] showed that the approximation should hold if the convolution of the parton densities is not very sensitive to the high η region.

3 Numerical results

In this section, we first test the applicability of our near-threshold treatment by calculating the parton luminosities. We then compare our approximate NNLO-NNLL cross sections with the exact NLO cross sections and the pp and $\pi^- p$ total charm cross sections. We also discuss the convergence properties and scale dependence of our results.

3.1 Parton luminosities

We first check if the parton luminosity peaks at low enough values of η for our near-threshold calculations to be applicable. Figures 1-3 show the parton luminosities for $\sqrt{S}$ = 6.98, 17.3 and 29.1 GeV respectively, corresponding to the top new GSI energy, the CERN SPS lead beam, and the SPS proton beam. The results are shown for three values of the charm quark mass at each energy: m = 1.2, 1.5 and 1.8 GeV. Using the lowest value of m gives relatively good agreement with pp data at NLO when $\mu = 2m$ [16, 17, 18]. This mass also represents a lower bound on the possible range of charm quark masses. The charm quark pole mass is most commonly chosen as 1.5 GeV. Finally, 1.8 GeV represents an upper bound on the charm mass.

The GRV 98 HO parton densities [19] are used in the luminosity calculations, shown with scales $\mu = m$ and $2m$. The scale is not decreased below m because the minimum scale in the parton densities is larger than $m/2$. Such calculations would thus be of little value.

Our results are primarily shown for the GRV 98 HO parton densities since they are consistent with the most recent pion parton densities by Glück, Reya and Schienbein [20], denoted here as GRS2. We will also compare our pp results with those using CTEQ5M [21] since these densities were used in our previous calculations for heavier quarks [13].

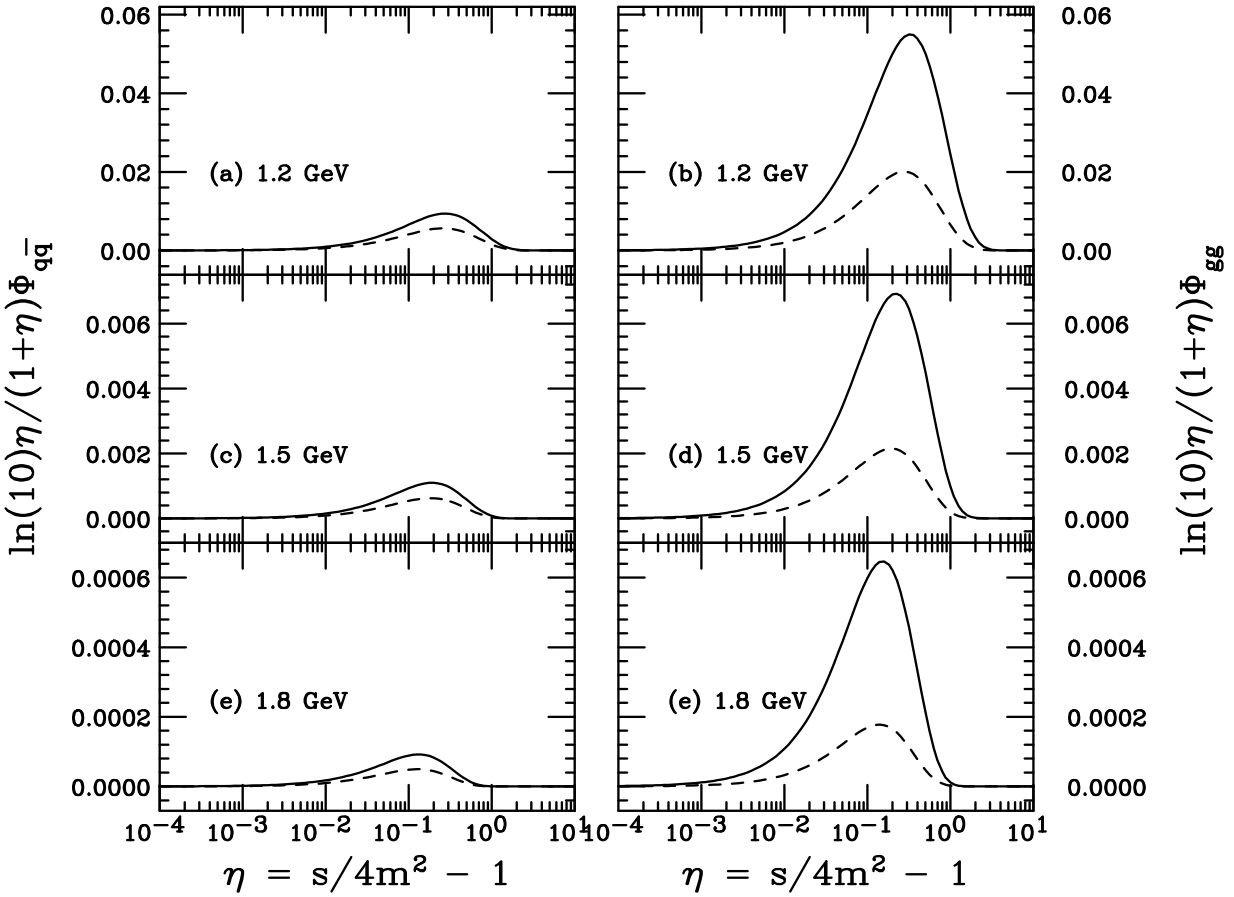

Figure 1: The parton luminosity for pp interactions at $\sqrt{S} = 6.98$ GeV as a function of η using the GRV 98 HO densities. The left-hand side gives the $q\overline{q}$ luminosity, the right-hand side the gg luminosity. From top to bottom, the charm quark mass is 1.2 GeV in (a) and (b), 1.5 GeV in (c) and (d), and 1.8 GeV in (e) and (f). The solid curves are with $\mu = m$ and the dashed, $\mu = 2m$.

At $\sqrt{S} = 6.98$ GeV, Fig. 1, charm production is well within the threshold region. There is no luminosity at $\eta > 2$ for $m = 1.5$ and 1.8 GeV while $\eta = 3$ is the highest η with nonzero luminosity for $m = 1.2$ GeV. It is interesting to note that at even this rather low energy, the gg luminosity is still the largest, nearly a factor of ten greater than the $q\overline{q}$ for $\mu = m$. The low $q\overline{q}$ luminosity can be attributed to the steeply falling antiquark density at large x, $\mu/\sqrt{S} \sim 0.2 - 0.6$, over the charm mass range considered here. Each step in m drops the luminosity by an order of magnitude while moving the peak to lower η, from $\eta \sim 0.35$ when $m = 1.2$ GeV to ~ 0.15 when $m = 1.8$ GeV. Increasing the scale decreases the gg luminosity by a factor of ≈ 3.

The luminosity is considerably higher at $\sqrt{S} = 17.3$ GeV, the Pb+Pb center of mass energy at the CERN SPS, as shown in Fig. 2. Now the peak in the luminosity is at higher η but still at $\eta < 1$, even for $m = 1.2$ GeV. Thus, charm production may still be considered as within the threshold region. The location of the peak in η is similar to that for $t\overline{t}$ production at the Tevatron [13]. Therefore, our calculations should be applicable. Changing the scale does not have a strong effect on the luminosity at this higher energy. The relative gg to $q\overline{q}$ luminosity

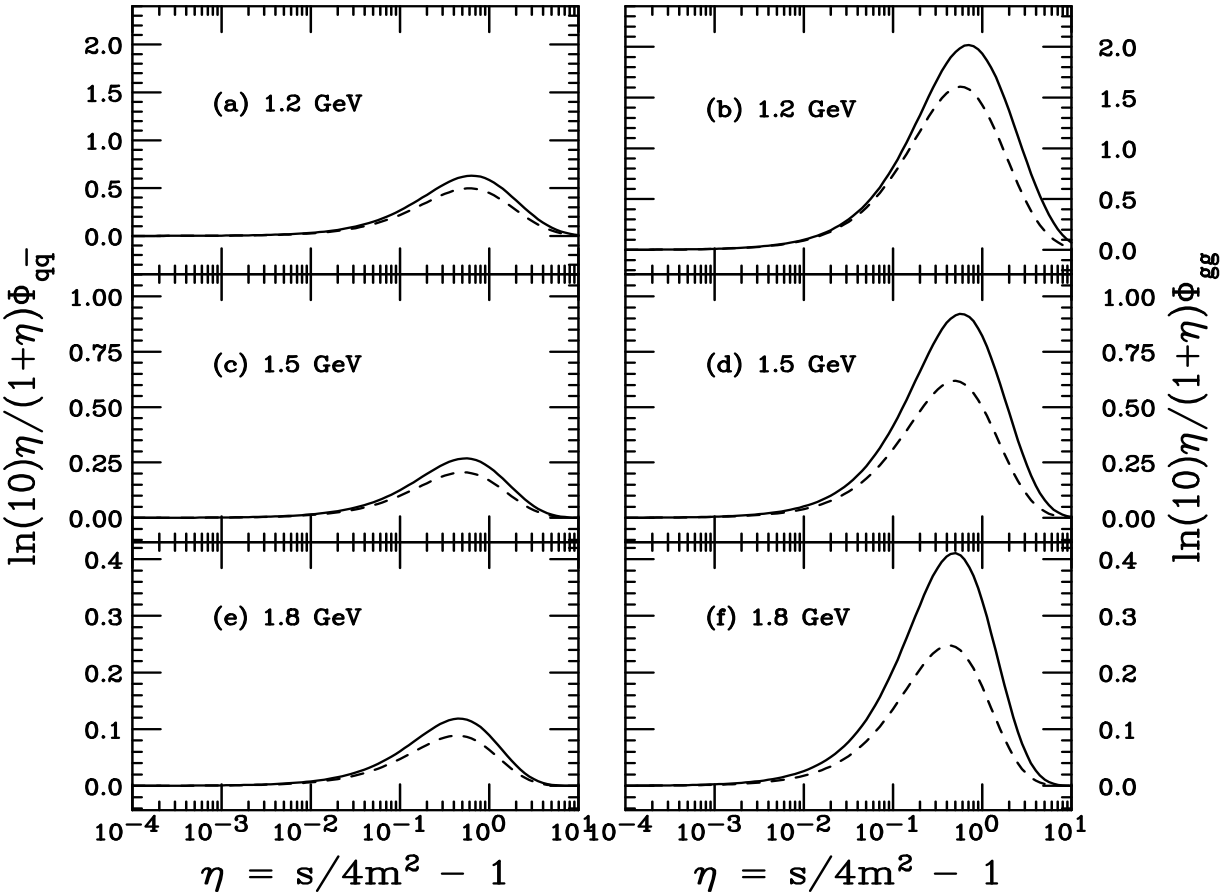

Figure 2: The parton luminosity for pp interactions at $\sqrt{S} = 17.3$ GeV as a function of η using the GRV 98 HO densities. The left-hand side gives the $q\overline{q}$ luminosity, the right-hand side the gg luminosity. From top to bottom, the charm quark mass is 1.2 GeV in (a) and (b), 1.5 GeV in (c) and (d), and 1.8 GeV in (e) and (f). The solid curves are with $\mu = m$ and the dashed, $\mu = 2m$.

is smaller than at the lower energy. The higher SPS proton center-of-mass energy, $\sqrt{S} = 29.1$ GeV, leads to a luminosity peak at somewhat larger η, but remains less than unity, see Fig. 3. Since some weight is given to the region $\eta \sim 10$, especially for the lowest m considered, this energy is the upper limit at which our calculation is applied.

While all the calculations shown in Figs. 1-3 have been made for the GRV 98 HO densities, the results for the CTEQ5M densities are quite similar. The luminosities in $\pi^- p$ interactions do differ however. At $\sqrt{S} = 6.98$ GeV, the $q\overline{q}$ luminosity is greater than the gg luminosity by a factor of ~ 1.5 for $m = 1.2$ GeV, increasing to nearly a factor of 5 for $m = 1.8$ GeV. By $\sqrt{S} = 17.3$ GeV, the situation has changed and the gg channel again dominates but only by a factor of 1.1-1.5. The smallest difference corresponds to the largest charm mass. Finally, at $\sqrt{S} = 29.1$ GeV, the $\pi^- p$ and pp luminosities are rather similar.

The scaling functions that contribute to the partonic cross section have been studied extensively in Ref. [13]. Since the scaling functions are essentially independent of m, we do not show them again here. We turn instead to a comparison of our calculations with the pp and $\pi^- p$ total charm cross section data.

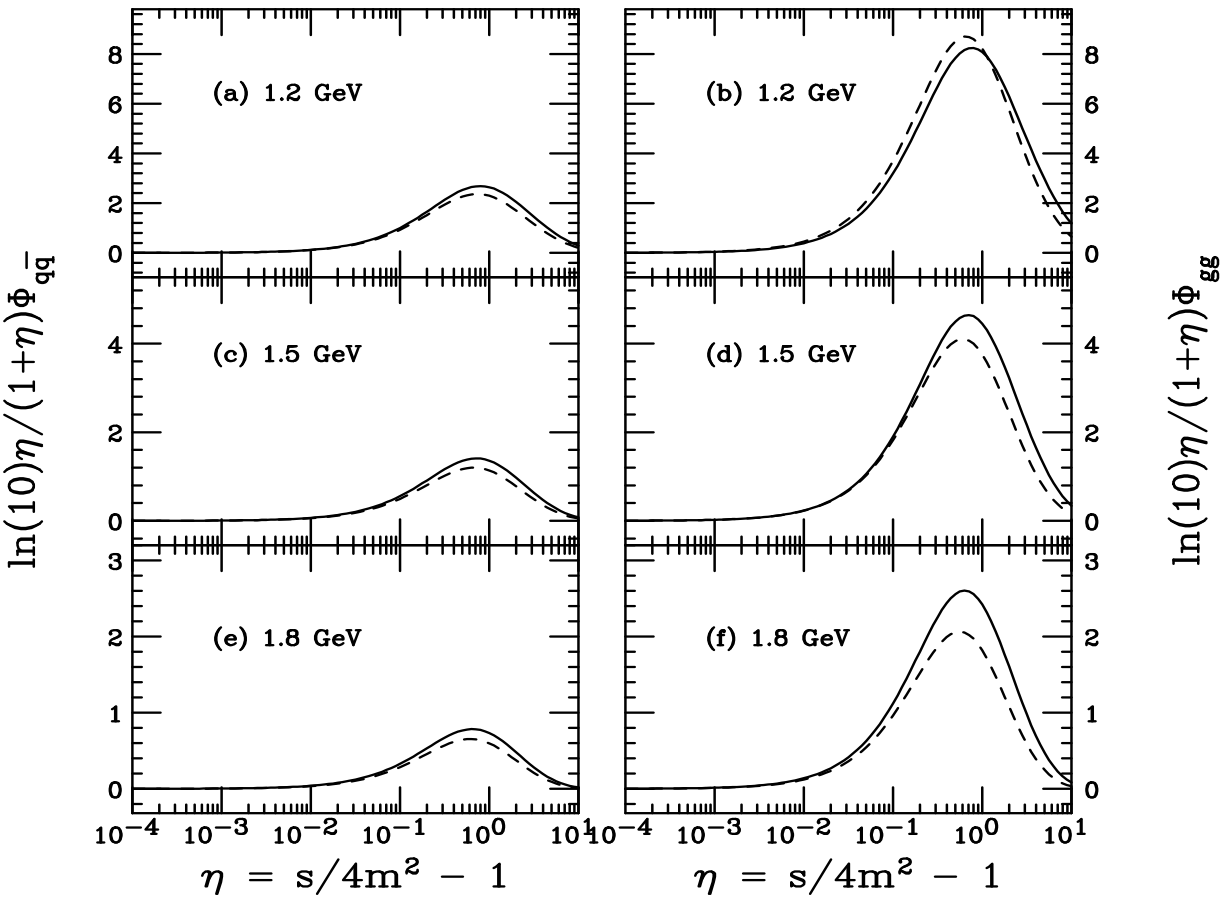

Figure 3: The parton luminosity for pp interactions at $\sqrt{S} = 29.1$ GeV as a function of η using the GRV 98 HO densities. The left-hand side gives the $q\overline{q}$ luminosity, the right-hand side the gg luminosity. From top to bottom, the charm quark mass is 1.2 GeV in (a) and (b), 1.5 GeV in (c) and (d), and 1.8 GeV in (e) and (f). The solid curves are with $\mu = m$ and the dashed, $\mu = 2m$.

3.2 Comparison with total charm data

Comparisons of the NLO cross sections to the available $c\overline{c}$ data have been made to obtain the 'best' agreement by eye with the data by varying the mass, m, and scale, μ, for several combinations of m, μ, and parton density [16, 17, 18]. The best agreement with data at NLO is with $\mu = m = 1.3$ GeV for the GRV 98 densities and with $\mu = m = 1.4$ GeV and $m = \mu/2 = 1.2$ GeV for CTEQ5M [18]. Thus the hadroproduction data tend to favor rather light charm masses.

We now turn to our NNLO-NNLL results. Since the NLO cross section is known exactly, we add the $\mathcal{O}(\alpha_s^4)$ NNLL approximate contribution to the exact NLO cross section in the $q\overline{q}$ and gg channels. We also apply a damping factor, $1/\sqrt{1+\eta}$, to temper the influence of the approximate scaling functions at large η where we are further from threshold and have less control over our approximations.

We find the greatest difference in the kinematics schemes for $\mu = m$. The effect of the NNLO-NNLL terms is reduced for higher scales because $\alpha_s(m) > \alpha_s(2m)$. The running of α_s is significant for charm because the mass is rather low. Thus the strong running of the coupling

constant for these values of μ ensures a large scale dependence for charm production. There is also a significant parton density dependence in the results because μ/Λ_3 is not large. Since $\Lambda_3 = 0.38$ GeV for CTEQ5M and 0.2475 GeV for GRV 98 HO, the NNLO-NNLL corrections will be larger for CTEQ5M than for GRV 98 HO.

The most important contribution to the NNLO-NNLL charm cross section is $f_{gg}^{(2,0)}$, shown in Fig. 5 of Ref. [13] for both 1PI and PIM kinematics. The differences between $f_{gg}^{(2,0)}$ in the two kinematics at large η are considerable. The functional dependence on η begins to diverge for $\eta > 0.1$. In 1PI kinematics, $f_{gg}^{(2,0)}$ is relatively small and positive until $\eta > 2$ when it begins to grow. On the other hand, in PIM kinematics $f_{gg}^{(2,0)}$ becomes large and negative with increasing η. This large negative contribution can sometimes lead to a negative total cross section for $\mu = m$ when the $\mathcal{O}(\alpha_s^4)$ contribution is larger than the NLO cross section. The decrease in α_s with $\mu = 2m$ keeps the total PIM cross section positive even though the NNLO-NNLL correction remains negative.

We note here that there is some arbitrariness in the functional form of the gg scaling functions since the expression $1 - 2t_1u_1/s^2$, used in the gg Born cross section in Ref. [13], is equivalent at threshold to $(t_1^2 + u_1^2)/s^2$. Either may be used in the scaling functions within the accuracy of our approximations. However, different choices can lead to non-trivial numerical differences in the cross section. We use the former choice here but point out that the latter choice increases the cross sections in both kinematics and leads to less negative (or even positive) values for the PIM results. We also note that including a class of subleading logarithms beyond NNLL, as derived in Ref. [12], considerably lessens the difference between the NNLO $q\overline{q}$ scaling functions in the two kinematics over a large η region. For the gg channel, especially given the ambiguity in the functional form of the gg scaling functions described above, it is harder to draw firm conclusions. A full evaluation of all the subleading terms requires two-loop calculations [22] and has not yet been done. However, the class of subleading logarithms arising from the inversion from moment to momentum space has been calculated exactly [12].

As is shown below, the NNLO-NNLL cross sections in the 1PI and PIM kinematics are very different. Since including the subleading logs seems to make the scaling functions more similar, especially in the $q\overline{q}$ channel, we are motivated to present results using the average of the two kinematics as well as the individual 1PI and PIM results in the remainder of the paper.

Our results with the GRV 98 HO densities are shown in Fig. 4 for pp interactions with both scales and the three charm quark masses. The approximate NNLO-NNLL cross sections are compared to the exact NLO results. We plot the 1PI and PIM cross sections as well as their average. The available data at $\sqrt{S} < 30$ GeV are included. In these figures, we are not attempting to fit the data but to show the effect of the $\mathcal{O}(\alpha_s^4)$ correction. The NNLO 1PI and PIM results with $\mu = m$ diverge most strongly from the NLO calculation. Increasing the charm mass reduces these differences, particularly for $\mu = 2m$. The PIM correction at NNLO-NNLL is larger and negative, giving a negative total cross section for $\mu = m = 1.2$ GeV.

The same trends are shown in Fig. 5 for the GRV 98 HO-based calculations of the total cross section in $\pi^- p$ interactions. We use the recently updated pion parton densities, GRS2 [20]. This evaluation has a somewhat lower gluon density than the previous GRV-π set [23].

We now show our pp results with CTEQ5M in Fig. 6. Since Λ_3 is larger for the CTEQ densities, all the cross sections are somewhat greater than those calculated with GRV 98 HO. The larger Λ_3 results in a larger α_s and hence larger higher-order corrections. The NNLO 1PI and PIM results with $\mu = m$ diverge most strongly from the NLO calculation. The PIM result for $m = 1.2$ GeV is already negative at $\sqrt{S} \sim 12$ GeV.

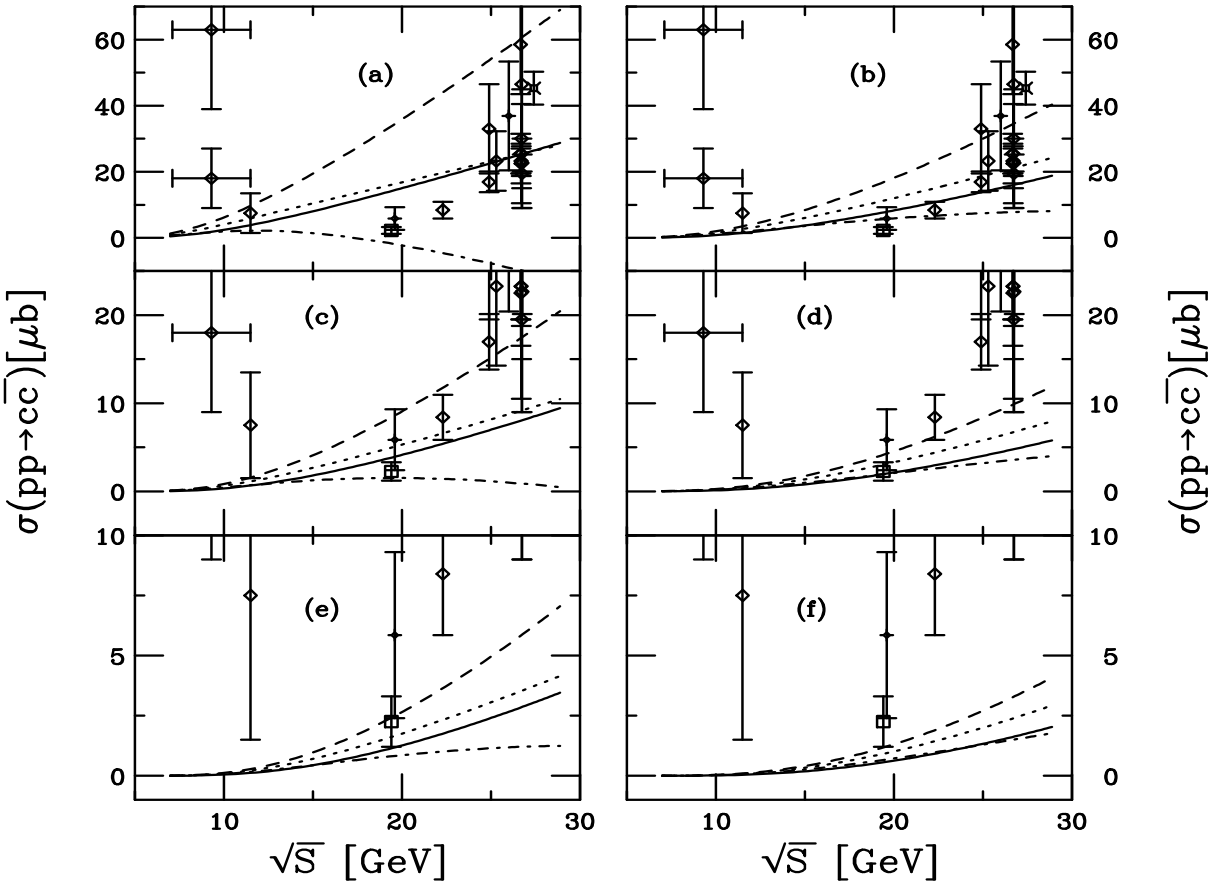

Figure 4: The total $c\overline{c}$ cross section in pp interactions as a function of $\sqrt{S}$ using the GRV 98 HO densities. The left-hand side employs the scale $\mu = m$, the right-hand side, $\mu = 2m$. From top to bottom, the charm quark mass is 1.2 GeV in (a) and (b), 1.5 GeV in (c) and (d), and 1.8 GeV in (e) and (f). The solid curves are the exact NLO result, the dashed curves, the approximate 1PI NNLO-NNLL result, the dot-dashed curves, the approximate PIM NNLO-NNLL result, and the dotted curves, the average of the 1PI and PIM NNLO-NNLL results.

The calculations agree only moderately well with the data. The earliest data are all rather low statistics and are mostly measurements of single D mesons. How the $c\overline{c}$ pairs hadronize is a particularly important question for energies near threshold where some channels may be energetically disfavored. We follow Ref. [7] and assume that since $\sigma(D_s)/\sigma(D^0 + D^+) \simeq 0.2$ and $\sigma(\Lambda_c)/\sigma(D^0 + D^+) \simeq 0.3$, it is possible to obtain the total $c\overline{c}$ cross section from $\sigma(D\overline{D})$ by multiplying it by ≈ 1.5. This assumption could have a strong energy dependence so that as many charm hadrons as possible should be measured at each energy to study hadronization. The fragmentation into $D\overline{D}$, $D\overline{\Lambda}_c$, $\Lambda_c\overline{D}$, $\Lambda_c\overline{\Lambda}_c$, *etc.* could be studied at the GSI facility if the experiments are able to reconstruct charm mesons and baryons.

Some of the total cross section data are based on lepton measurements. Semileptonic decays do not allow the momentum of the primary D meson to be entirely reconstructed, adding an additional layer of experimental uncertainty. The CERN SPS results are based on muon spectrometers which cannot unambiguously determine the identity of the primary hadron. Finally, some of the data are taken on nuclear targets and then extrapolated to pp assuming that the

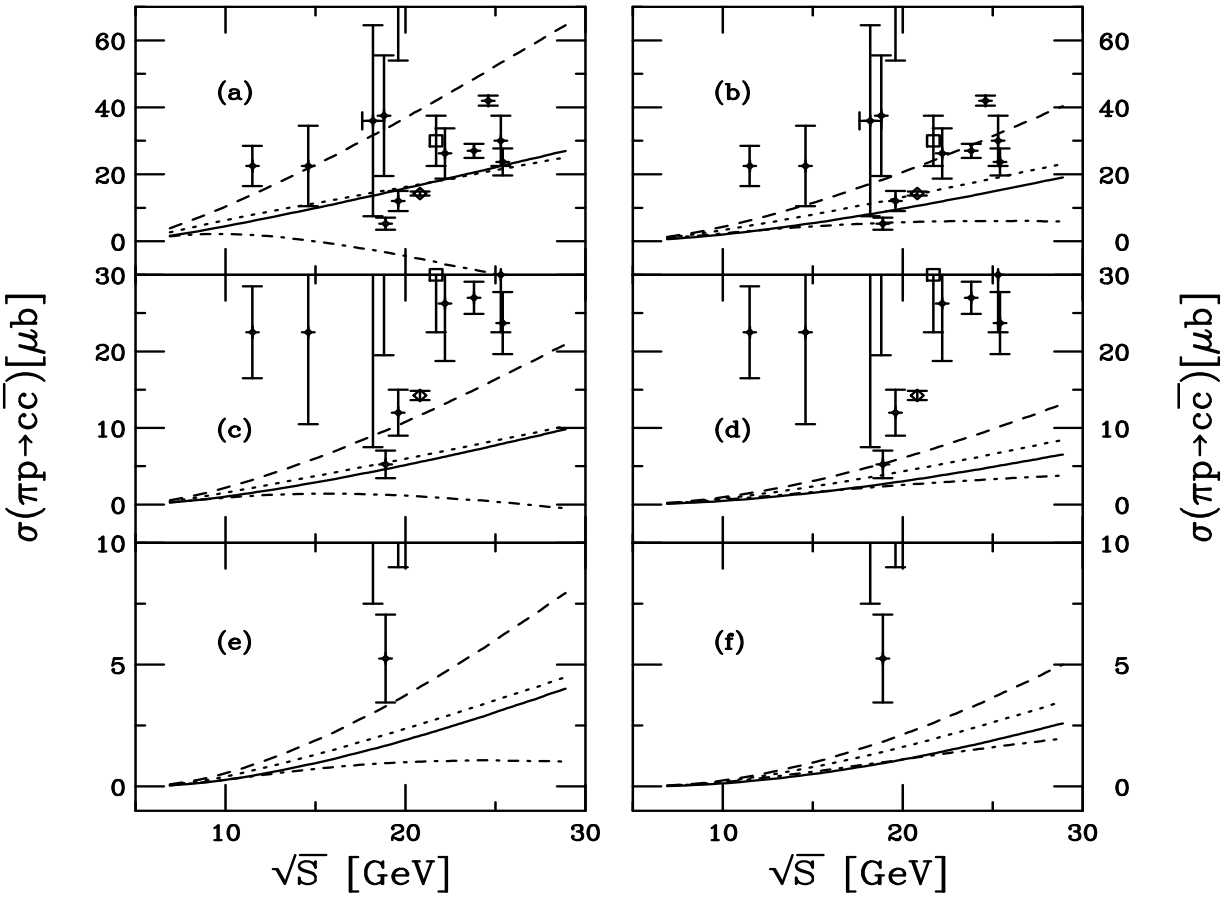

Figure 5: The total $c\bar{c}$ cross section in $\pi^- p$ interactions as a function of $\sqrt{S}$ using the GRV 98 HO proton densities and the GRS2 pion densities. The left-hand side employs the scale $\mu = m$, the right-hand side, $\mu = 2m$. From top to bottom, the charm quark mass is 1.2 GeV in (a) and (b), 1.5 GeV in (c) and (d), and 1.8 GeV in (e) and (f). The solid curves are the exact NLO result, the dashed curves, the approximate 1PI NNLO-NNLL result, the dot-dashed curves, the approximate PIM NNLO-NNLL result, and the dotted curves, the average of the 1PI and PIM NNLO-NNLL results.

cross sections scale linearly with A, supported by fixed target measurements of the A dependence of charm production [25]. Thus the placing of data on the plots is primarily to guide the eye.

The total cross sections in pp interactions for the three energies we have discussed are given in Table 1. The scale dependence is not necessarily reduced at NNLO-NNLL relative to the exact NLO. Due to the complete dominance of the gg channel in pp interactions, the dependence on kinematics choice is large. Because $f_{gg}^{(2,0)}$ grows with η at large η in 1PI kinematics, the 1PI cross section is always larger than the NLO exact result. On the other hand, the PIM result always underestimates the exact NLO calculation since $f_{gg}^{(2,0)}$ is large and negative at large η in PIM kinematics. Thus the PIM cross section with $\mu = 2m$ can be greater than that with $\mu = m$. The average of the 1PI and PIM cross sections typically remains somewhat above the NLO result.

Recall that all the results include the damping factor. Without the damping factor, the $\mathcal{O}(\alpha_s^4)$ contribution can increase up to 40% at the highest energies.

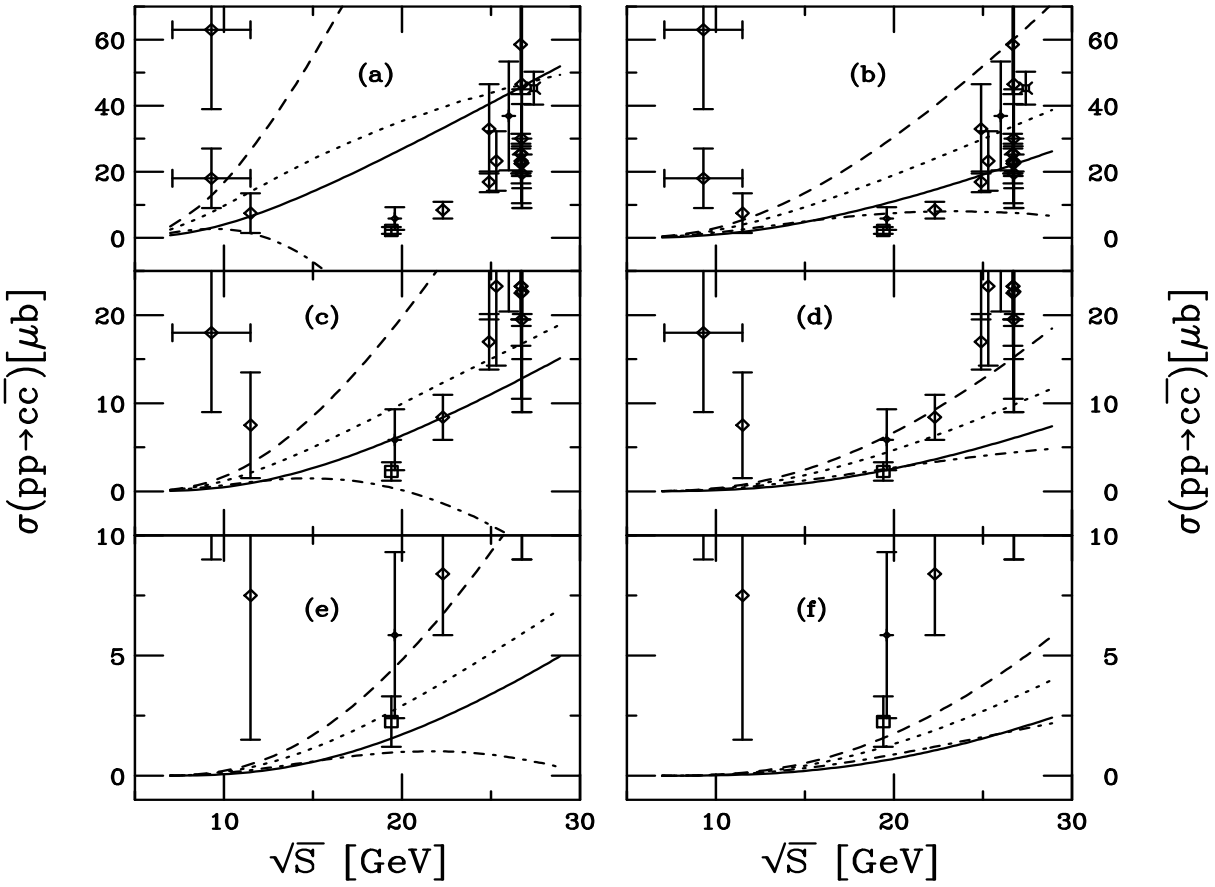

Figure 6: The total $c\bar{c}$ cross section in pp interactions as a function of $\sqrt{S}$ using the CTEQ5M densities. The left-hand side employs the scale $\mu = m$, the right-hand side, $\mu = 2m$. From top to bottom, the charm quark mass is 1.2 GeV in (a) and (b), 1.5 GeV in (c) and (d), and 1.8 GeV in (e) and (f). The solid curves are the exact NLO result, the dashed curves, the approximate 1PI NNLO-NNLL result, the dot-dashed curves, the approximate PIM NNLO-NNLL result, and the dotted curves, the average of the 1PI and PIM NNLO-NNLL results.

Note that even for the NLO exact cross section, the CTEQ5M results are larger than the GRV 98 HO results. Because Λ_3 is greater for CTEQ5M, the NNLO-NNLL corrections will be most important for this set. The dependence on parton densities is reduced for heavier quarks since the ratio $\mu/\Lambda \gg 1$ and a change in the ratio will not affect the value of α_s significantly for large μ. That is a primary reason why the scale dependence is small for top quark production [12, 13]. In this case, the running of α_s is primarily responsible for the dependence of the results on parton density and the large kinematics dependence.

As discussed before, attempts to find agreement with the pp and $\pi^- p$ charm production data by varying the mass and scale usually result in a rather low value of m at NLO, ≈ 1.2 GeV for $\mu = 2m$. The NNLO-NNLL results, particularly with 1PI kinematics, suggest that the same general energy dependence may be obtained for higher masses and lower scales so that a value of m closer to the pole mass, 1.5 GeV, would agree with the fixed target data. Using the GRV 98 HO densities, the NLO calculation with $m = 1.2$ GeV and $\mu = 2m$ is in reasonable agreement with the approximate NNLO-NNLL 1PI result obtained with $\mu = m = 1.5$ GeV.

Even at NNLO-NNLL, $m = 1.8$ GeV still underestimates the data considerably.

Finally, we briefly compare our finite order result to the NLL-resummed result for $pp \to c\overline{c}$ shown in Fig. 15 of Ref. [11]. Note that the resummed cross section depends on the prescription used to obtain the momentum space result. Our NLO calculations with $m = 1.5$ GeV and CTEQ5M are in good agreement with their NLO calculation using MRSR2 [24] since these two sets have similar values of Λ. The NLL resummed cross section, calculated using the partonic total cross sections, is in rather good agreement with our kinematics-averaged NNLO-NNLL results.

3.3 Convergence properties

Given the large corrections at NNLO-NNLL, one can question if the calculated cross section will stabilize such that all data can be described with one value of the charm mass even if NNNLO and higher order corrections were calculated. Since the NNLO-NNLL 1PI results allow the data to be described relatively well with $\mu = m = 1.5$ GeV instead of $m = 1.2$ GeV and $\mu = 2m$, it is quite possible that further corrections could lead to agreement with the data for still higher values of m. We can at least partially address this issue through an investigation of the K factors.

We first briefly discuss the calculation of the 'first order K factor', $K^{(1)} = \sigma_{\rm NLO}/\sigma_{\rm LO}$. Since $\sigma_{\rm LO}$ can be calculated with LO or NLO parton densities, the value of the K factor depends on which way $\sigma_{\rm LO}$ is calculated. In Ref. [26], $K^{(1)}$ was defined in three ways. We compare two of the definitions here: $K_0^{(1)}$, where $\sigma_{\rm LO}$ is calculated with NLO parton densities and a two-loop evaluation of α_s, and $K_2^{(1)}$, where $\sigma_{\rm LO}$ is calculated with LO parton densities and a one-loop evaluation of α_s. In both cases, the Born and $\mathcal{O}(\alpha_s^3)$ contributions to $\sigma_{\rm NLO}$ are calculated with NLO parton densities and two-loop evaluations of α_s. The first definition, $K_0^{(1)}$, indicates the convergence of terms in a fixed-order calculation while the second, $K_2^{(1)}$, indicates the convergence of the hadronic calculation towards a result. If $K_0^{(1)} > K_2^{(1)}$, the convergence of the hadronic cross section is more likely.

In Fig. 7, we compare $K_0^{(1)}$ and $K_2^{(1)}$ for charm production in pp interactions with the GRV 98 HO densities. The dotted curves are $K_0^{(1)}$ and the solid curves are $K_2^{(1)}$. Here, $K_0^{(1)} > K_2^{(1)}$ for all values of μ and m shown. We see that for $\mu = m$, $K_2^{(1)}$ does not change much with m. It is ≈ 3.5 for $\sqrt{S} = 6.98$ GeV, decreasing to ≈ 1.9 at $\sqrt{S} = 29.1$ GeV for all cases. There is slightly more change with m for $\mu = 2m$ since $K_2^{(1)}$ tends to flatten at lower $\sqrt{S}$ with increasing mass. At higher $\sqrt{S}$, $K_2^{(1)}$ is somewhat bigger for the larger scale, ≈ 2.2. On the other hand, $K_0^{(1)}$ is a stronger function of both μ and m. When $\mu = m$, $K_0^{(1)}$ increases from ≈ 3.7 for $m = 1.2$ GeV to 4.2 for $m = 1.8$ GeV at $\sqrt{S} = 6.98$ GeV, decreasing to ≈ 2.2 for higher $\sqrt{S}$. When $\mu = 2m$, $K_0^{(1)}$ increases 10-15%.

If, instead, we use the CTEQ5M densities to calculate the NLO K factors in pp interactions, $K_2^{(1)} > K_0^{(1)}$ at all energies and the values are all larger than for the GRV 98 HO densities. The larger K factors for CTEQ5M are due to the larger α_s with the CTEQ5M Λ_3.

More interesting are the K factors in $\pi^- p$ interactions, shown in Fig. 8. With the GRV 98 HO densities, again $K_0^{(1)} > K_2^{(1)}$ for all μ and m but the values are much smaller and almost independent of energy. When $\mu = m$, $K_2^{(1)} \approx 1.5$ and $K_0^{(1)} \approx 2.2$ while when $\mu = 2m$, $K_2^{(1)} \approx 2$ and $K_0^{(1)} \approx 2.5$. Both the reduced size of the K factors as well as their near energy independence can be attributed to the greater importance of $q\overline{q}$ annihilation in charm production, particularly

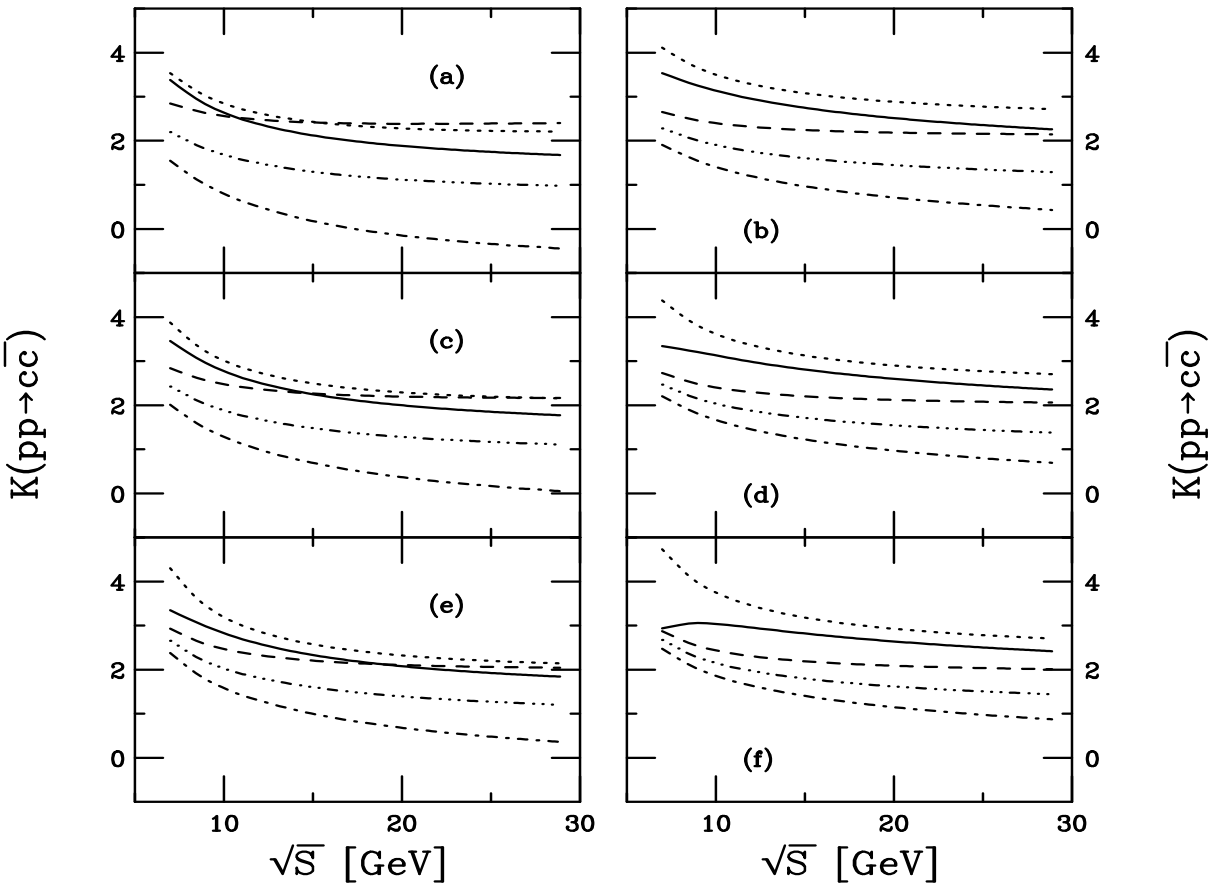

Figure 7: The theoretical K factors for $c\overline{c}$ production in pp interactions as a function of $\sqrt{S}$ using the GRV 98 HO densities. The left-hand side employs the scale $\mu = m$, the right-hand side, $\mu = 2m$. From top to bottom, the charm quark mass is 1.2 GeV in (a) and (b), 1.5 GeV in (c) and (d), and 1.8 GeV in (e) and (f). The solid curves are $K_2^{(1)}$, the dotted curves, $K_0^{(1)}$, the dashed curves, $K_{\rm 1PI}^{(2)}$, the dot-dashed, $K_{\rm PIM}^{(2)}$, and the triple dot-dashed, $K_{\rm ave}^{(2)}$, as defined in the text.

at low $\sqrt{S}$. The $\mathcal{O}(\alpha_s^3)$ contribution to the $q\overline{q}$ channel is considerably smaller relative to $\sigma_{\rm LO}$ than in the gg channel, reducing the K factor. Since the pp cross sections are dominated by the gg channel, their K factor is always large.

All these NLO K factors are rather large for pp interactions, typically a factor of two or more. We can define the next order K factor, $K^{(2)} = \sigma_{\rm NNLO-NNLL}/\sigma_{\rm NLO}$, and see if it is reduced relative to $K^{(1)}$. We define $K_{\rm 1PI}^{(2)}$, where the NNLO-NNLL 1PI cross section is in the numerator, $K_{\rm PIM}^{(2)}$, with the PIM cross section in the numerator, and $K_{\rm ave}^{(2)}$ where the numerator is the average of the 1PI and PIM cross sections. We cannot distinguish between calculations with parton densities at different orders for these K factors, as we did for $K^{(1)}$, because there are no full NNLO parton densities available. Now both numerator and denominator are calculated with all NLO parton densities and the two-loop evaluation of α_s. By calculating $K^{(2)}$ for the NLO parton densities, we can identify improvements in the fixed-order results relative to $K_0^{(1)}$.

Figure 7 also shows $K_{\rm 1PI}^{(2)}$, $K_{\rm PIM}^{(2)}$ and $K_{\rm ave}^{(2)}$ in the dashed, dot-dashed and triple dot-dashed curves respectively. The 1PI K factor, $K_{\rm 1PI}^{(2)}$, is not strongly dependent on μ, m or $\sqrt{S}$. It

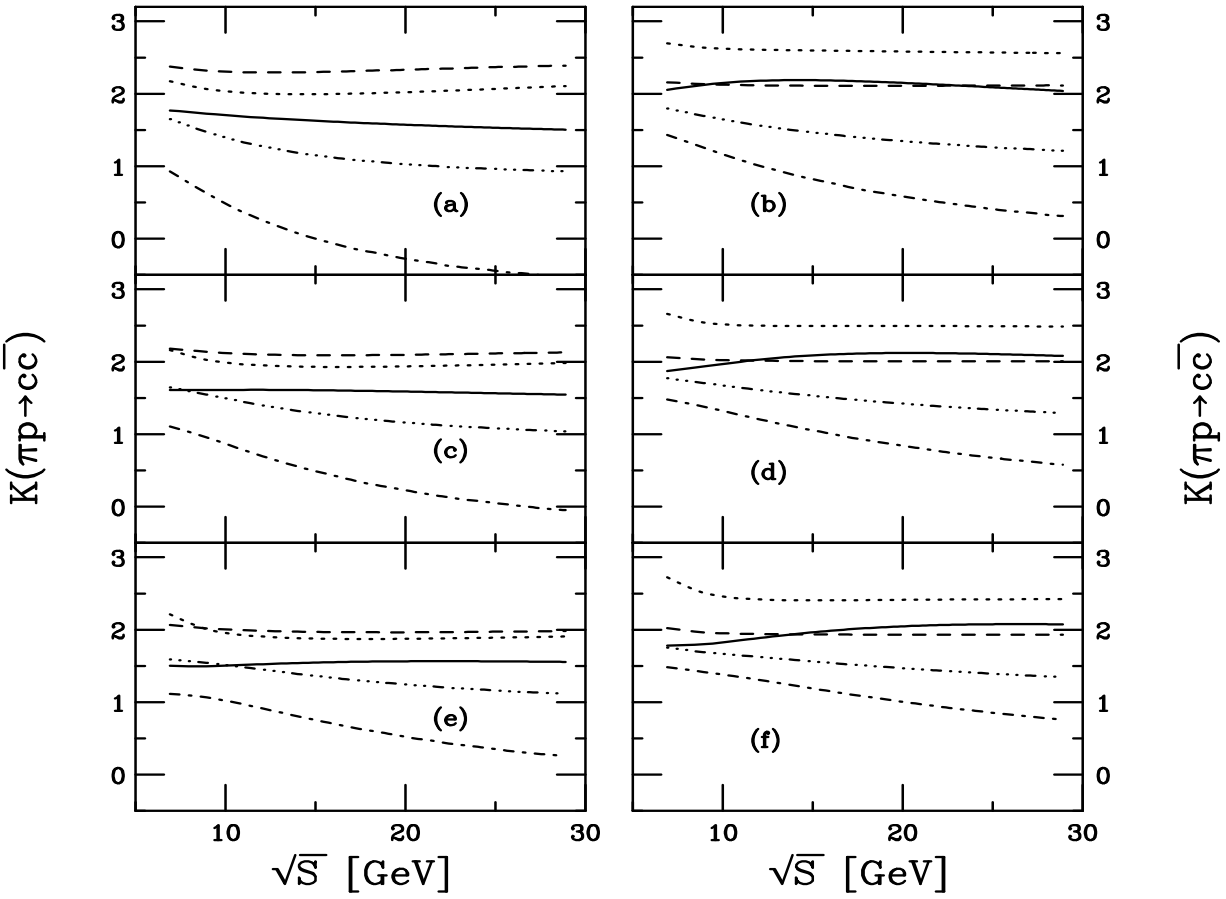

Figure 8: The theoretical K factors for $c\overline{c}$ production in $\pi^- p$ interactions as a function of $\sqrt{S}$ using the GRV 98 HO proton densities and the GRS2 pion densities. The left-hand side employs the scale $\mu = m$, the right-hand side, $\mu = 2m$. From top to bottom, the charm quark mass is 1.2 GeV in (a) and (b), 1.5 GeV in (c) and (d), and 1.8 GeV in (e) and (f). The solid curves are $K_2^{(1)}$, the dotted curves, $K_0^{(1)}$, the dashed curves, $K_{\rm 1PI}^{(2)}$, the dot-dashed, $K_{\rm PIM}^{(2)}$, and the triple dot-dashed, $K_{\rm ave}^{(2)}$, as defined in the text.

decreases slowly from ≈ 3 at low $\sqrt{S}$ to ≈ 2 at higher $\sqrt{S}$. Consequently for $\mu = m$, it is smaller than either calculation of $K^{(1)}$ at low $\sqrt{S}$ and larger than $K^{(1)}$ as we move out of the threshold region. When $\mu = 2m$, $K_{\rm 1PI}^{(2)}$ is always less than $K^{(1)}$. However, $K_{\rm PIM}^{(2)}$ has the strongest μ, m and $\sqrt{S}$ dependence of all the K factors even though it is the smallest. The fact that it is smaller is less indicative of the ultimate convergence of the expansion than of the fact that the NNLO-NNLL PIM contribution to the cross section is large and negative. This is demonstrated by the change of $K_{\rm PIM}^{(2)}$ from positive to negative for $\sqrt{S} > 17$ GeV when $\mu = m = 1.2$ GeV. As the charm mass increases, the slope of $K_{\rm PIM}^{(2)}$ with $\sqrt{S}$ decreases and the K factor remains positive. The average K factor, $K_{\rm ave}^{(2)}$, is less than both $K_0^{(1)}$ and $K_2^{(1)}$ everywhere. It remains positive and is not strongly dependent on m, μ or $\sqrt{S}$, remaining $\sim 2-3$ at low $\sqrt{S}$ and decreasing to ~ 1 at higher $\sqrt{S}$.

Similar trends are observed for the CTEQ5M densities but now the $K^{(2)}$ factors are all larger and more dependent on μ and m, even $K_{\rm 1PI}^{(2)}$. Now also $K_{\rm PIM}^{(2)} < 0$ for $\mu = m = 1.2$ GeV and 1.5 GeV at large $\sqrt{S}$. For $\pi^- p$ interactions, on the other hand, all the K factors are again

smaller and $K_{\rm 1PI}^{(2)}$ is almost independent of energy, as shown in Fig. 8.

We could form another K factor, $K^{(2')} = \sigma_{\rm NNLO-NNLL}/\sigma_{\rm LO} = K^{(2)}K_2^{(1)}$, to test the convergence of the hadronic cross section. The result is not complete because the NNLO-NNLL cross section is only approximate and the NNLO parton densities are unavailable. By multiplying the K factors shown in Fig. 7, we see that $K_{\rm 1PI}^{(2')}$ is ≈ 10 at low $\sqrt{S}$ and $\approx 4-5$ at larger $\sqrt{S}$. Note that $K_{\rm ave}^{(2')}$ is smaller and $K_{\rm ave}^{(2')} \sim K_2^{(1)}$ at high $\sqrt{S}$. It is difficult to tell from these results if further, higher order, K factors such as $\sigma_{\rm NNNLO}/\sigma_{\rm NNLO-NNLL}$ will be consistently smaller than 2 near threshold or not. The convergence of the hadronic cross section at low scales is thus left in doubt although we note that subleading terms may have some effect on the convergence properties of the cross section [12]. Since $K^{(2)} < K_2^{(1)}$ for $\mu = 2m$, one can expect that the next-order correction might be still smaller but this is not certain. In any case, it is not a guarantee that even larger masses may be needed to obtain the by-eye agreement at NLO with further higher-order corrections.

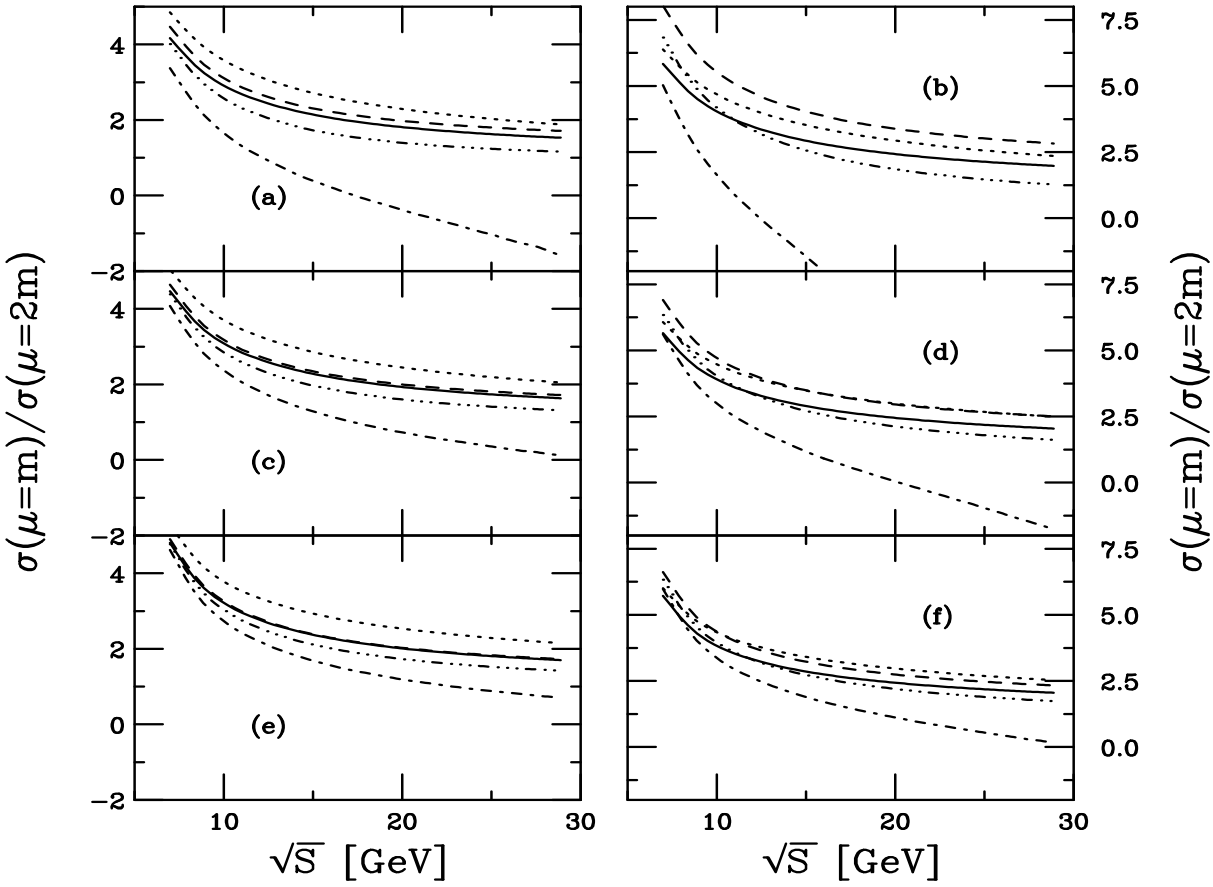

Figure 9: The scale dependence of $c\bar{c}$ production in pp interactions as a function of $\sqrt{S}$. The left-hand side employs the GRV 98 HO parton densities, the right-hand side, CTEQ5M. From top to bottom, the charm quark mass is 1.2 GeV in (a) and (b), 1.5 GeV in (c) and (d), and 1.8 GeV in (e) and (f). The LO (dotted), NLO (solid), NNLO-NNLL 1PI (dashed), NNLO-NNLL PIM (dot-dashed) and the 1PI-PIM average (triple dot-dashed) ratios are shown.

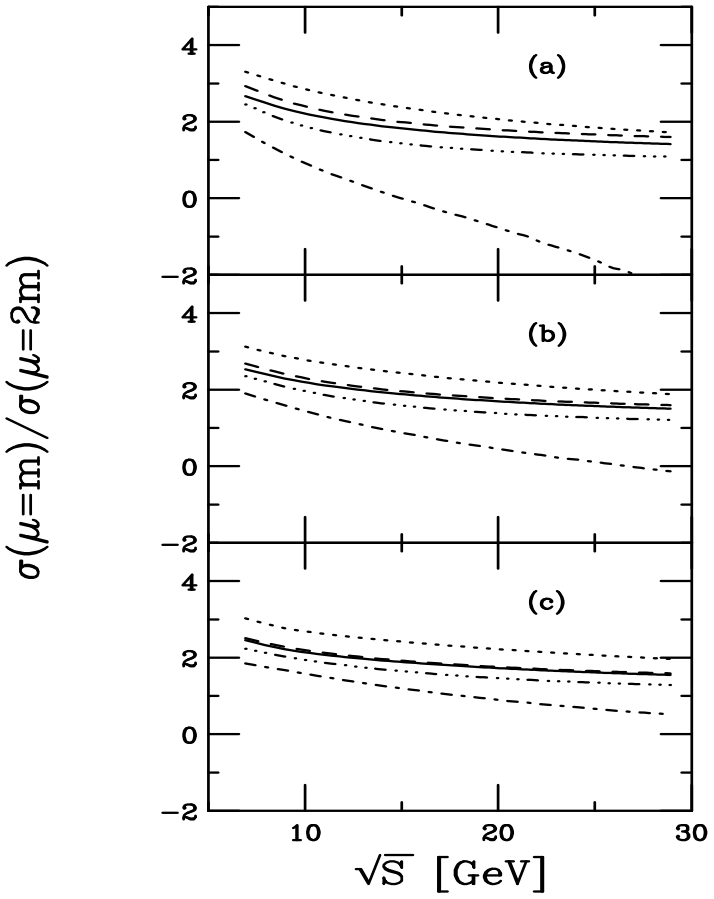

Figure 10: The scale dependence of $c\overline{c}$ production in $\pi^- p$ interactions as a function of $\sqrt{S}$, using the GRV 98 HO proton densities and the GRS2 pion densities. From top to bottom, the charm quark mass is 1.2 GeV in (a) and (b), 1.5 GeV in (c) and (d), and 1.8 GeV in (e) and (f). The LO (dotted), NLO (solid), NNLO-NNLL 1PI (dashed), NNLO-NNLL PIM (dot-dashed) and the 1PI-PIM average (triple dot-dashed) ratios are shown.

3.4 Scale dependence

We now turn to a comparison of the scale dependence at LO, NLO and NNLO-NNLL, shown in Fig. 9 for the ratio $\sigma(\mu = m)/\sigma(\mu = 2m)$ as a function of $\sqrt{S}$ in pp interactions. The GRV 98 HO scale dependence is shown on the left-hand side and the CTEQ5M scale dependence on the right-hand side. The GRV 98 HO scale dependence is largest for the LO ratio. The NNLO-NNLL 1PI ratio is somewhat larger than the NLO ratio for $m = 1.2$ GeV but the two are almost identical for $m = 1.8$ GeV. Thus for 1PI, the scale dependence is not reduced relative to NLO but it is not really increased either. The NNLO-NNLL PIM ratio is smaller than the other ratios but it is a stronger function of energy, again becoming negative for $m = 1.2$ GeV as $\sqrt{S}$ increases. This ratio has the largest mass dependence. The ratio for the average of the NNLO-NNLL 1PI and PIM cross sections remains below the NLO ratio for all energies shown.

The CTEQ5M scale dependence is considerably larger. In this case, when $m = 1.2$ GeV, the NNLO-NNLL 1PI scale dependence is larger even than the LO, dropping below it only when $m = 1.8$ GeV. The overall increase in the scale dependence relative to GRV 98 HO is again related to the larger α_s for low scales with the CTEQ densities which also increases the

NNLO-NNLL contribution to the total cross section.

The scale dependence of $\pi^- p$ production, shown in Fig. 10, is considerably reduced and, except for the NNLO-NNLL PIM ratio, nearly independent of energy. This reduction in the scale dependence can again be attributed to the relatively larger $q\overline{q}$ contribution to the total cross section.

4 Conclusions

We have studied the behavior of NNLO-NNLL calculations for charm production near threshold in pp and $\pi^- p$ interactions in both 1PI and PIM kinematics. We find that there are large differences in the results for different kinematics. Thus, the uncertainties in the cross sections remain large even at NNLO-NNLL. There are additional uncertainties, mentioned earlier, due to the functional form of the scaling functions and to subleading logarithms which have some effect on the values and convergence of the 1PI and PIM cross sections. We note that the average of the 1PI and PIM results has some nice properties such as better convergence and less scale dependence. For both pp and $\pi^- p$ interactions, either choice of scale, and all values of $\sqrt{S}$ (except when $\mu = m = 1.2$ GeV at high $\sqrt{S}$) , the average of the NNLO-NNLL 1PI and PIM results lies above the NLO cross section. Thus, the charm mass need not be too low to agree with the data. However the poor convergence properties as well as other uncertainties of the 1PI and PIM results make any quantitative statement about the inclusive charm hadroproduction cross section difficult.

Acknowledgments

The research of N.K. has been supported by a Marie Curie Fellowship of the European Community programme "Improving Human Research Potential" under contract number HPMF-CT-2001-01221. The work of E.L. is supported by the Foundation for Fundamental Research of Matter (FOM) and the National Organization for Scientific Research (NWO). The work of R.V. is supported in part by the Division of Nuclear Physics of the Office of High Energy and Nuclear Physics of the U.S. Department of Energy under Contract No. DE-AC-03-76SF00098.

References

[1] M.C. Abreu *et al.* (NA50 Collab.), Eur. Phys. J. C**14**, 443 (2000).

[2] L. Grandchamp and R. Rapp, Phys. Lett. B**523**, 60 (2001).

[3] M.I. Gorenstein, A.P. Kostyuk, H. Stöcker and W. Greiner, Phys. Lett. B**509**, 277 (2001); J. Phys. G**27**, L47 (2001).

[4] M.I. Gorenstein, A.P. Kostyuk, H. Stöcker and W. Greiner, arXiv:hep-ph/0012292.

[5] A. Baldit *et al.* (NA60 Collab.), Proposal SPSC/P316, March 2000; see http://na60.web.cern.ch/NA60 for more details.

[6] For plans for the future facility, see the GSI home page, http://www.gsi.de.

[7] S. Frixione, M.L. Mangano, P. Nason and G. Ridolfi, Nucl. Phys. B**431**, 453 (1994).

[8] N. Kidonakis and G. Sterman, Phys. Lett. B**387**, 867 (1996); Nucl. Phys. B**505**, 321 (1997).

[9] N. Kidonakis, G. Oderda, and G. Sterman, Nucl. Phys. **B525**, 299 (1998); **B531**, 365 (1998).

[10] J. Smith and R. Vogt, Z. Phys. C**75**, 271 (1997).

[11] R. Bonciani, S. Catani, M.L. Mangano and P. Nason, Nucl. Phys. B **529**, 424 (1998)

[12] N. Kidonakis, Phys. Rev. D**64**, 014009 (2001).

[13] N. Kidonakis, E. Laenen, S. Moch, and R. Vogt, Phys. Rev. D**64**, 114001 (2001); in proceedings of Quark Matter '02, arXiv:hep-ph/0208119.

[14] W. Beenakker, H. Kuijf, W. L. van Neerven, and J. Smith, Phys. Rev. D **40**, 54 (1989).

[15] W. Beenakker, W. L. van Neerven, R. Meng, G. A. Schuler, and J. Smith, Nucl. Phys. **B351**, 507 (1991).

[16] P.L. McGaughey *et al.*, Int. J. Mod. Phys. A**10**, 2999 (1995).

[17] R. Vogt, to appear in the Proceedings of the Hard Probe Collaboration, LBNL-45350, arXiv:hep-ph/0111271.

[18] R. Vogt, in *Proc. of the 18*$^{\rm th}$ *Winter Workshop on Nuclear Dynamics*, eds. R. Bellwied *et al.*, Nassau, The Bahamas, 2002, p. 253, arXiv:hep-ph/0203151.

[19] M. Glück, E. Reya and A. Vogt, Eur. Phys. J. C**5**, 461 (1998).

[20] M. Glück, E. Reya and I. Schienbein, Eur. Phys. J. C**10**, 313 (1999).

[21] H.L. Lai *et al.*, Eur. Phys. J. C**12**, 375 (2000).

[22] N. Kidonakis, arXiv:hep-ph/0208056; in *DPF2002*, arXiv:hep-ph/0207142.

[23] M. Glück, E. Reya and A. Vogt, Z. Phys. C**53**, 651 (1992).

[24] A.D. Martin, R.G. Roberts and W.J. Stirling, Phys. Lett. **B387**, 419 (1996).

[25] G.A. Alves *et al.* (E769 Collab.), Phys. Rev. Lett. **70**, 722 (1993).

[26] R. Vogt, Heavy Ion Phys. in press, arXiv:hep-ph/0207359.

	σ(NLO) (μb)		σ(1PI) (μb)		σ(PIM) (μb)	
$\sqrt{S}$ (GeV)	$\mu = m$	$\mu = 2m$	$\mu = m$	$\mu = 2m$	$\mu = m$	$\mu = 2m$
$m = 1.2$ GeV						
GRV 98 HO						
6.98	0.45	0.11	1.29	0.29	0.70	0.21
17.3	11.1	5.61	26.5	12.4	0.075	4.71
29.1	28.8	18.8	69.0	40.3	-12.9	8.09
CTEQ5M						
6.98	0.76	0.13	3.50	0.44	1.48	0.29
17.3	19.5	7.33	75.5	20.5	-17.0	6.32
29.1	51.9	26.2	200.1	70.7	-101.4	6.66
$m = 1.5$ GeV						
GRV 98 HO						
6.98	0.028	0.0062	0.079	0.017	0.056	0.014
17.3	2.75	1.31	6.13	2.83	1.44	1.44
29.1	9.44	5.77	20.4	11.9	0.47	4.00
CTEQ5M						
6.98	0.043	0.0077	0.17	0.025	0.11	0.019
17.3	4.13	1.55	13.1	4.08	1.19	1.86
29.1	15.1	7.37	46.3	18.5	-8.50	4.82
$m = 1.8$ GeV						
GRV 98 HO						
6.98	0.0014	0.00030	0.0042	0.00086	0.0034	0.00074
17.3	0.76	0.35	1.63	0.74	0.63	0.44
29.1	3.45	2.13	7.05	4.08	1.24	1.77
CTEQ5M						
6.98	0.0024	0.00042	0.0094	0.0014	0.0070	0.0012
17.3	1.01	0.38	2.89	0.97	0.82	0.54
29.1	4.97	2.42	13.5	5.79	0.32	2.18

Table 1: Charm total cross sections in pp interactions at the three fixed target energies considered. The results are given for the NLO exact, the 1PI and PIM NNLO-NNLL approximate cross sections. The $c\overline{c}$ cross sections using the GRV 98 HO and CTEQ5M parton densities are compared.